Quantifying the relative importance of direct and indirect biophysical effects of deforestation on surface temperature and teleconnections

N. Devaraju, Nathalie de Noblet-Ducoudré, Benjamin Quesada, G. Bala

Quantifying the Relative Importance of Direct and Indirect Biophysical Effects of Deforestation on Surface Temperature and Teleconnections

N. DEVARAJU AND NATHALIE DE NOBLET-DUCOUDRÉ

Laboratoire des Sciences du Climat et de l'Environnement/IPSL, Unité mixte CEA-CNRS-UVSQ, Université Paris-Saclay, Gif-sur-Yvette, France

BENJAMIN QUESADA

Institute of Meteorology and Climate Research, Atmospheric Environmental Research, Karlsruhe Institute of Technology, Garmisch-Partenkirchen, Germany

G. BALA

Centre for Atmospheric and Oceanic Sciences, Indian Institute of Science, Bangalore, India

(Manuscript received 25 August 2017, in final form 5 February 2018)

ABSTRACT

In this study, the authors linearize the surface energy budget equation that disentangles indirect effects (resulting from changes in downward shortwave and longwave radiation and air temperature) from direct biophysical effects (resulting from changes in surface albedo, evapotranspiration, and roughness length) of deforestation on land surface temperature. This formulation is applied to idealized deforestation simulations from two climate models and to realistic land-use and land-cover change (LULCC) simulations from 11 models, and the contribution of each underlying mechanism to surface temperature change is quantified. It is found that the boreal region experiences dominant indirect effects and the tropics experience dominant direct effects in all seasons in idealized deforestation simulations. The temperate region response differs in the two models. However, five out of seven models in response to realistic historical LULCC show a dominance of indirect effects in the temperate region. In response to future LULCC, three out of four models confirm the dominance of direct effects in the tropical region. It is found that indirect effects are always largely attributable to air temperature feedback and direct effects are essentially driven by changes in roughness length in both idealized and realistic simulations. Furthermore, teleconnections are shown to exist between deforested regions and the rest of the world, associated with the indirect effects. The study also shows that the partitioning between direct and indirect effects is highly model dependent, which may explain part of the intermodel spread found in previous studies comparing the total biophysical effects across models.

1. Introduction

The response of climate to biophysical effects of land-use-induced land-cover change (LULCC) is highly heterogeneous and can either be warming or cooling depending on the location of change and the land cover transition. Many observational (Lee et al. 2011; Luyssaert et al. 2014; Li et al. 2015; Alkama and Cescatti 2016; Khanna et al. 2017) and modeling studies on LULCC effects (Bala et al. 2007; Betts et al. 2007; Davin and de Noblet-Ducoudré 2010; Bright et al. 2015; Li et al. 2016) have identified that the main contributors to the temperature responses are changes in albedo, evapotranspiration efficiency, and surface roughness. These changes in land surface properties, linked to soil and vegetation characteristics, trigger both direct and indirect effects (Davin and de Noblet-Ducoudré 2010). The term direct effects is used when changes in surface temperature occur via alteration of absorbed solar

Denotes content that is immediately available upon publication as open access.

Supplemental information related to this paper is available at the Journals Online website: https://doi.org/10.1175/JCLI-D-17-0563.s1.

Corresponding author: N. Devaraju, devaraju.narayanappa@lsce.ipsl.fr

DOI: 10.1175/JCLI-D-17-0563.1

radiation due to albedo changes and perturbations to the partitioning of net radiation due to changes in evapotranspiration efficiency and roughness length (Pielke et al. 2011; Chen and Dirmeyer 2016, hereafter CD16). When a change in surface temperature occurs via changes in the air temperature (resulting from changes in circulation and snow cover) and incoming radiation (resulting from changes in humidity and clouds), we refer to this as indirect effects (Boisier et al. 2012). In this study, we quantify the extent to which both direct and indirect effects of LULCC contribute to surface temperature change, within and outside the deforested regions.

The dominant biophysical process in the northern high latitudes for a conversion from forests to crops or grassland is the change in albedo, which increases the reflection of solar radiation and causes cooling at the surface (one of the direct effects; Fig. 1a) (Lee et al. 2011; Bathiany et al. 2010; Bonan 2002). As cooler surface temperatures help maintain snow on the ground, the larger reflection of a snowy ground amplifies the initial cooling via air temperature feedback (an indirect effect; Fig. 1b) (Betts 2001). In the tropics, although the direct effect of albedo change also induces cooling, its magnitude is smaller than in high latitudes as there is no contribution of the snow-albedo feedback. The dominant biophysical process in such conditions is the reduction in roughness length for grasslands compared to forests. This reduction induces a shallower planetary boundary layer, which causes a reduced vertical turbulent transport of energy from the surface to the atmosphere, leading to surface warming (Fig. 1c; Baldocchi and Ma 2013; McNaughton and Spriggs 1986; Barr and Betts 1997).

Moreover, for conversion from forests to grasslands, evapotranspiration efficiency reduces because of shallow-rooted grasslands and their smaller leaf area index (Bonan 2008; Davin and de Noblet-Ducoudré 2010; Pielke et al. 2011; Lawrence and Vandecar 2015). Latent heat flux is much smaller over grasslands and hence the conversion contributes not only to surface warming but also to the drying of the lower atmosphere. The decrease in atmospheric water vapor lowers downwelling longwave radiation (Fig. 1f), thereby partly dampening the warming. On the other hand, the decreased atmospheric humidity leads to a reduction in cloudiness, which in turn increases downwelling shortwave radiation (Fig. 1d) and warms the land surface. Further, depending on the location of deforestation, an increase (decrease) of the Bowen ratio is associated with an increase (decrease) in the temperature at the surface (Fig. 1e).

Atmospheric circulation changes may also triggered by direct and indirect LULCC effects that then affect the regions far away from the initial tree cover change (Snyder et al. 2004; Medvigy et al. 2012; Mahmood et al. 2014; Winckler et al. 2017). For instance, increased subsidence over tropical forests resulting from decreased turbulent exchanges between land and atmosphere may be compensated for by increased ascending air elsewhere. Recent studies (Swann et al. 2012; Devaraju et al. 2015; Laguë and Swann 2016) have shown that LULCC in boreal and midlatitude regions can modify the global energy balance, impacting cloud cover, precipitation, and circulation patterns in distant regions through atmospheric teleconnections. The total changes over the deforested locations (combining direct and indirect effects) are referred to as local effects. Our analysis also explores the temperature change outside the deforested locations (teleconnections or remote effects) arising from direct and indirect LULCC effects.

To decompose the direct and indirect effects on surface temperature, an energy budget equation is used on pairs of simulations with and without LULCC (see section 2b). Decomposition of the two effects is also possible by comparing forced land surface simulations (generally called ''offline'') to coupled land–atmosphere–ocean simulations (generally called ''online''). Offline simulations do not account for indirect effects from the atmosphere, whether local or remote, whereas the atmosphere in online simulations interacts with the land surface (and with the ocean), and hence both direct and indirect effects are simulated. Subtracting offline from online results gives the indirect effects. However, performing both types of simulations consumes more processor time and also many climate models are not yet able to run the identical version of their land surface models uncoupled from the atmosphere. Hence, decomposition of the surface energy budget equation is more efficient for inferring the relative contributions of the direct and indirect effects.

The decomposition of energy budget equation has been tested in both observational and modeling studies (Lee et al. 2011; Luyssaert et al. 2014; Vanden Broucke et al. 2015; CD16). For example, Lee et al. (2011) assumes zero atmospheric feedbacks and investigates only the direct effects. Luyssaert et al. (2014) and Vanden Broucke et al. (2015) have not distinguished direct and indirect effects but only separated the incident radiation and the turbulent fluxes on surface temperature using paired FLUXNET sites data over forests and open land sites. CD16 demonstrate the usefulness of the two methods: 1) an extension of Lee et al. (2011) to account for atmospheric feedbacks and 2) the method used by Luyssaert et al. (2014). However, to our knowledge no other study, except CD16, has quantified the direct and indirect effects using a single metric. Our study goes

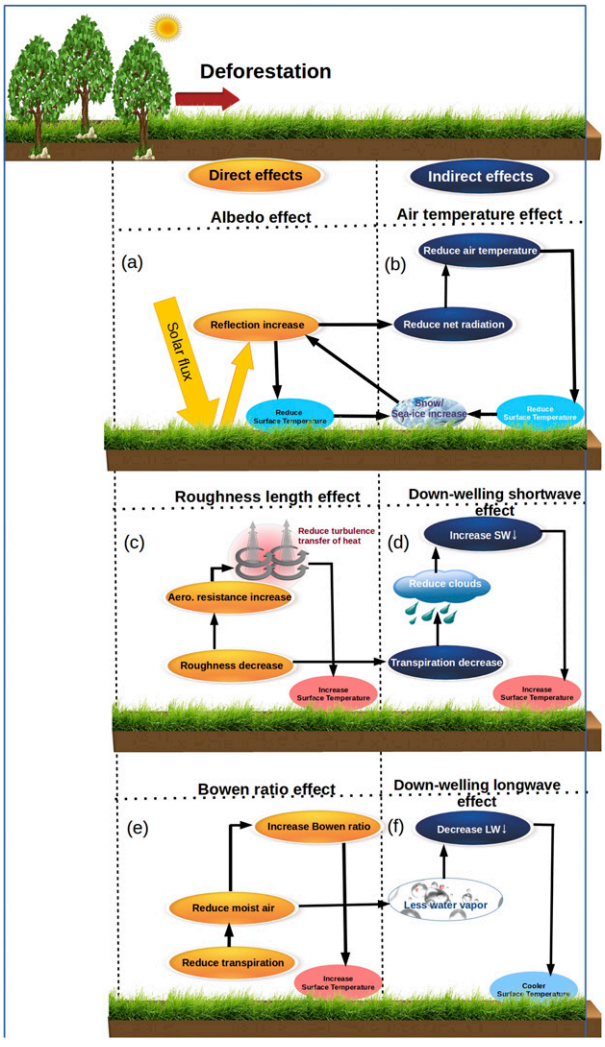

FIG. 1. Schematic diagram illustrating the direct and indirect effects of deforestation on surface temperature. Direct effect result from changes to (a) albedo, (c) roughness length, and (e) Bowen ratio while indirect effects are due to feedbacks from sea ice/snow albedo, water vapor, cloud, lapse rate, and soil moisture. In this study, for indirect effects, we focus on three integrated feedback effects through changes in (b) air temperature and in downwelling (d) shortwave and (f) longwave radiation. Note that the schematic illustrates some of the important processes of deforestation. For example, the Bowen ratio effect illustrated in the schematic (e) is one characteristic in a particular region in response to deforestation. The decrease in latent heat does not necessarily lead to higher surface temperature. The changes in the Bowen ratio can be either positive or negative in response to deforestation depending on the location of deforestation.

beyond CD16 and identifies (i) the full indirect effects for not only idealized simulations but also more realistic historical and future ones, (ii) which latitudinal deforested band (tropical, temperate, or boreal) triggers the largest direct or indirect effects, and through which dominant process, and (iii) the intermodel spread of the partitioning between direct and indirect effects across multiple models. Furthermore, observational sites are not large enough to capture large-scale indirect feedback effects; this is possible only through fully coupled simulations (CD16; Vanden Broucke et al. 2015; Zhang et al. 2014). Hence, we use fully coupled climate system models to investigate the relative importance of direct and indirect LULCC effects and their teleconnection effects at the biome and global scale.

In section 2, we describe the Earth system models used to perform experiments, list the available simulations, and formulate the method for disentangling direct and indirect effects. In section 3, the contributions of various direct and indirect effects to simulated surface temperature change from idealized deforestation and realistic LULCC simulations are discussed. The results are summarized and discussed in section 4.

2. Experiments, models, and methods

a. Experiments and models

1) IDEALIZED DEFORESTATION SIMULATIONS

We perform four large-scale idealized deforestation simulations over 1) the whole globe (GLOBAL), 2) the boreal band (BOREAL), 3) the temperate band (TEMPERATE), and 4) the tropical band (TROPICAL), using L'Institut Pierre-Simon Laplace Coupled Model, version 5 (IPSL-CM5). The selection of biome latitudinal band cutoffs (provided below) for this model follows a protocol designed within the European research project Earth System Model Bias Reduction and Assessing Abrupt Climate Change (EMBRACE; http://www.embrace-project.eu). A similar set of deforestation simulations using the Community Earth System Model, version 1.0.2 (CESM1.0), was available from Devaraju et al. (2015), but with minor differences in resolution, latitudinal bands for biomes, and the number of simulation years (provided below). The spatial distribution of tree plant functional types (PFTs) on average is nearly similar in both models except in the Southeast Asia region (see Fig. S1 in the supplemental material), but the PFT area per latitudinal band is not identical. In the deforestation simulations tree PFTs are converted to grasslands in both the models.

(i) IPSL-CM5

We use the latest version of IPSL-CM5, which is composed of the ORCHIDEE land surface model, version 5 of the LMDZ atmosphere model (LMDZv5), and the NEMO ocean model (Dufresne et al. 2013). IPSL-CM5 participated in the latest phase of the

Coupled Model Intercomparison Project [phase 5 of CMIP (CMIP5)] and is referred to as IPSL-CM5A-LR. A horizontal resolution of 1.9° latitude × 3.8° longitude, with 39 levels in the vertical and a time step of 30 min, is used. The leaf area index is prognostic in the land surface model and sea surface temperatures (SSTs) are calculated interactively. The model is first run for more than 400 years as a spinup with 1850 levels of CO_2 concentration (284.7 ppm), non-CO_2 greenhouse gases, ozone, aerosols, and PFT map [control simulation (CTL): the last 30 years are used for the analysis). Using the restart files from the end of the spun up CTL simulation as the initial conditions, the deforestation simulations are performed. The deforested areas in this model for GLOBAL, BOREAL (45°–90°N), TEMPERATE (everything south of 23°S and 23°–45°N), and TROPICAL (23°S–23°N) cases are 78.9, 23.6, 18.8, and 23.6 × 10^6 km^2, respectively. The deforestation simulations typically reach equilibrium in about 20 years, and all simulations last for 50 years. For the analysis we use only the last 30 years of monthly output data and the first 20 years are discarded as model spinup.

(ii) CESM1.0

This model consists of the Community Atmosphere Model, version 5.0 (CAM5.0; Neale et al. 2012) coupled to the Community Land Model, version 4 (CLM4; Mullens 2013) and a slab ocean model (SOM). The minor differences in CESM1.0 compared to IPSL-CM5 simulations are the following: the horizontal resolution is 1.9° latitude × 2.5° longitude and 27 levels in the vertical, the BOREAL deforestation band is 50°–90°N, the TEMPERATE deforestation band is 50°–20°S and 20°–50°N, and the TROPICAL deforestation band is 20°S–20°N. Deforested areas are 53.3, 13.7, 15.3, and 23.1 × 10^6 km^2 for the GLOBAL, BOREAL, TEMPERATE, and TROPICAL deforestation cases, respectively. The deforestation simulations along with CTL simulation are run for 80 years; the first 30 years are discarded as model spinup, and the last 50 years of monthly output are used for the analysis.

The minor difference in latitudinal bands for the BOREAL, TEMPERATE, and TROPICAL simulations between IPSL-CM5 and CESM1.0 is unlikely to alter our findings in this study. Although the deforested areas per latitudinal band are not similar in the two models, we find very small changes in surface temperature due to different latitudinal band cutoffs (see Table S1 in the supplemental material). Analyses are done for each model on their own resolutions. The number of simulation years is not similar in the two models because the time taken to reach climate equilibrium is different in the two models; also, because the models are developed by different groups. However, the global mean drift (slope of the linear regression) in steady-state conditions (the last 50 years in CESM1.0 and the last 30 years in IPSL-CM5) are about the same in the two models (~0.01 K), so the use of different number of years is unlikely to alter the conclusions reached in this study. The idealized large-scale deforestation simulations in coupled models can help us to understand the sensitivity of the atmospheric state to changes in land and the regional distribution of the sensitivity. It is also easier to evaluate the differing sensitivity of the climate models to LULCC. Furthermore, idealized simulations allow a larger signal-to-noise ratio compared to realistic LULCC scenarios.

2) REALISTIC SIMULATIONS OF PAST AND FUTURE LULCC

(i) LUCID simulations

To understand the effects of historical LULCC (twentieth century) relative to preindustrial vegetation cover (set at 1870), we use the Land-Use and Climate, Identification of Robust Impacts (LUCID) simulations, which are described in Pitman et al. (2009) and de Noblet- Ducoudré et al. (2012). The LUCID project is a major international intercomparison exercise to diagnose the robust biophysical impacts of LULCC using as many climate models as possible forced with same LULCC (http://www.lucidproject.org.au/). In this project, four types of simulations are performed by seven global climate models (GCMs) to evaluate the impact of LULCC from the preindustrial period to present day [see Boisier et al. (2012) for more details]. The preindustrial (PI) and present-day (PD) experiments are forced with prescribed data (SST, sea ice cover, atmospheric CO_2 concentrations, and land-cover maps) for the periods 1870–99 and 1970–99, respectively. Another experiment (PDv) was also performed using the present-day conditions but with vegetation cover corresponding to the preindustrial period. Finally, experiment PIv is performed using the preindustrial conditions but with the present-day vegetation (for the year 1992). Thus, the biophysical effect of LULCC between 1870 and 1992 is calculated as 0.5 × (PD − PDv + PIv − PI). All simulations were run in an ensemble mode (five members per model ensemble) to provide more robustness, hence improved confidence in the results reported (see Boisier et al. 2012).

(ii) LUCID-CMIP5 simulations

To understand the effects of future LULCC, we use LUCID-CMIP5 simulations as described in Brovkin et al. (2013). Here, we use data from four LUCID-CMIP5 coupled models (CanESM2, IPSL-CM5A-LR, MPI-ESM-LR, and HadGEM2-ES). Two simulations

from these four models are analyzed: 1) the representative concentration pathway 8.5 (RCP8.5) simulation as prescribed in the CMIP5 protocol and LULCC varies from year to year (Riahi et al. 2011) and 2) the L2A85 simulation, which is the same as RCP8.5 but without LULCC (land cover data corresponds to the year 2005). The difference RCP8.5 − L2A85 will separate out the biophysical effects of future LULCC. Analyzed data here correspond to the last 30-yr period of each experiment (2071–2100). We interpolate the output to an intermediate resolution for our analysis because of different resolutions of the model simulations in both LUCID and LUCID-CMIP5 experiments. We assume interpolation to a single resolution does not significantly affect the partitioning of direct and indirect effects in these model simulations.

All of our model simulations (both idealized and realistic) do not account for carbon–climate interaction after LULCC; hence, in this study we do not assess LULCC effects on CO_2 emissions and their effects on the radiative forcing and consequently on surface temperature change (also called biochemical effects). We investigate only direct and indirect biophysical effects of LULCC in this study.

b. *Decomposition method for surface temperature change*

To decompose the simulated surface temperature change into direct and indirect changes, we use the surface energy budget equation. Many previous studies also make use of this equation for decomposing the net effect into individual biophysical effects (Juang et al. 2007; Lee et al. 2011; Luyssaert et al. 2014; Thiery et al. 2015).

The surface energy budget equation at equilibrium is given by

$$(1-\alpha_s)\mathrm{SW}_{\downarrow} + \mathrm{LW}_{\downarrow} - \varepsilon\sigma T_s^4 = H + \mathrm{LE} + G, \quad (1)$$

where α_s is the surface albedo (unitless), $\mathrm{SW}_{\downarrow}$ is downwelling shortwave radiation ($\mathrm{W\,m^{-2}}$), $\mathrm{LW}_{\downarrow}$ is downwelling longwave radiation ($\mathrm{W\,m^{-2}}$), ε is surface emissivity (unitless), σ is the Stephan–Boltzmann constant ($\mathrm{W\,m^{-2}\,K^{-4}}$), T_s is surface temperature (K), H is the sensible heat flux ($\mathrm{W\,m^{-2}}$), LE is the latent heat flux ($\mathrm{W\,m^{-2}}$), and G is the ground heat flux ($\mathrm{W\,m^{-2}}$). Multiyear mean (seasonal and annual) G changes are very small after deforestation in both the models (not shown); hence we neglect G in the following analysis. Substituting for LE using the Bowen ratio $\beta = H/\mathrm{LE}$ and for H using $H = \rho C_p(T_s - T_a)/r_a$ in Eq. (1), where ρ is the density of air ($\mathrm{kg\,m^{-3}}$), C_p is the specific heat constant ($\mathrm{J\,kg^{-1}\,K^{-1}}$), r_a is the aerodynamic resistance ($\mathrm{s\,m^{-1}}$) and T_a is air temperature at 2 m (K; hereafter simply called air temperature), and reordering the terms yields the following:

$$\varepsilon\sigma T_s^4 = (1-\alpha)\mathrm{SW}_{\downarrow} + \mathrm{LW}_{\downarrow} - \frac{(1+\beta)}{\beta}\frac{\rho C_p}{r_a}(T_s - T_a). \quad (2)$$

Taking the first-order derivative of Eq. (2) and rearranging its terms (see section S1 in the supplemental material for more details), we get the difference in surface temperature ΔT_s between deforestation and control simulations:

$$\begin{aligned}\Delta T_s = {} & \underbrace{\left(\frac{-\lambda_0 \mathrm{SW}_{\downarrow}}{1+f}\right)}_{\mathrm{I}}\Delta\alpha + \underbrace{\left[\frac{\lambda_0 H}{(1+f)\beta^2}\right]}_{\mathrm{II}}\Delta\beta \\ & + \underbrace{\left[\frac{fH}{(1+f)\rho C_p}\right]}_{\mathrm{III}}\Delta r_a + \underbrace{\left[\frac{\lambda_0(1-\alpha)}{1+f}\right]}_{\mathrm{IV}}\Delta\mathrm{SW}_{\downarrow} \\ & + \underbrace{\left(\frac{\lambda_0}{1+f}\right)}_{\mathrm{V}}\Delta\mathrm{LW}_{\downarrow} + \underbrace{\left(\frac{f}{1+f}\right)}_{\mathrm{VI}}\Delta T_a \text{ and} \\ \Delta T_s = {} & \Delta\mathrm{Ts}_{\mathrm{direct}} + \Delta\mathrm{Ts}_{\mathrm{indirect}},\end{aligned} \quad (3)$$

where $\Delta\mathrm{Ts}_{\mathrm{direct}} = \mathrm{I} + \mathrm{II} + \mathrm{III}$ and $\Delta\mathrm{Ts}_{\mathrm{indirect}} = \mathrm{IV} + \mathrm{V} + \mathrm{VI}$, and

$$\lambda_0 = \frac{1}{4\sigma\varepsilon T_s^3} \quad \text{and} \quad f = \frac{\rho C_p}{4\sigma\varepsilon T_s^3 r_a}\left(1 + \frac{1}{\beta}\right).$$

The right-hand side (RHS) terms of Eq. (3) represent the individual factors of direct (terms I–III) and indirect (terms IV–VI) effects on the surface temperature change (see Fig. 1): term I for albedo change, term II for Bowen ratio change, term III for roughness length change, term IV for downwelling shortwave radiation change, term V for downwelling longwave radiation change, and term VI for air temperature change. The parameters in the coefficient are the temperature sensitivity λ_0 and the energy redistribution efficiency f [as discussed in Lee et al. (2011)]. In our calculation of direct effect, the Bowen ratio is calculated as $\beta = H/\mathrm{LE}$ and r_a is calculated as $r_a = \rho C_p(T_s - T_a)/H$ (Zhao et al. 2014; CD16). Also, Eq. (3) can be written exactly as Eq. (S14) in Lee et al. (2011) by assigning $\Delta T_a = 0$, $\Delta\mathrm{LW}_{\downarrow} = 0$, and $\Delta\mathrm{SW}_{\downarrow} = 0$ (absence of indirect effects) and using Eq. (S7) of Lee et al. (2011).

Term I in Eq. (3) clearly implies that an increase in albedo due to deforestation decreases surface temperature (Fig. 1a), and term II indicates that if β increases, then surface temperature increases as well. Note that β may either decrease or increase following deforestation; ΔT_s will then decrease or increase depending on the

location of deforestation. Increases in β could correspond to decreases in evapotranspiration and to warming (Fig. 1e). The inverse relation to β^2 means that $\Delta\beta$ has a large contribution to ΔT_s in tropical climates, where β is typically small (e.g., $\beta = 0.3$; von Randow et al. 2004) and a negligible contribution in semiarid climate (e.g., $\beta = 6.6$; Rotenberg and Yakir 2011; Lee et al. 2011). The roughness length change term III implies that an increase in aerodynamic resistance ($\Delta r_a > 0$, resulting from decrease in roughness length) after deforestation increases surface temperature because of reduced turbulent transfer of heat from the surface (Fig. 1c). The downwelling shortwave and longwave feedback terms IV and V, in essence, represent an integrated measure of respective indirect feedbacks from water vapor, clouds, lapse rate, and potential teleconnections. These two terms (IV and V) essentially indicate that increases in incoming shortwave radiation (fewer clouds) after deforestation warms the surface (Fig. 1d), whereas the decrease in downwelling longwave radiation (less water vapor) after deforestation cools the surface (Fig. 1f). The last term, term VI, connects the change in boundary layer temperature (ΔT_a) to a subsequent change in the surface temperature (ΔT_s) with an efficiency factor f. Warmer air will warm the surface. Finally, the sum of all six terms on the RHS of Eq. (3) represents the total surface temperature change between deforestation experiments and the control simulation in a fully coupled mode. We caution that this equation is valid for multiyear time scales only, because we assume no change in ground storage heat flux.

c. *Significance test*

The significance level (with 95% confidence) for the changes in spatial distribution is estimated using the modified Student's t test based on Zwiers and von Storch (1995) and the false discovery rate (FDR; Wilks 2006) field significance test with 50 samples of seasonal mean differences in CESM1.0 and 30 samples of seasonal mean differences in IPSL-CM5. The modified Student's t test takes into account autocorrelation in time and reduces to the standard Student's t test if the data are not autocorrelated. The FDR is used to account for the fact that we apply the modified Student's t test multiple times in space (at every grid point) and correlation in space [following Lorenz et al. (2016) and Pitman and Lorenz (2016)].

3. Results

a. *Idealized simulation results*

In this section, we present results from the idealized deforestation simulations. The simulated results for GLOBAL, BOREAL, TEMPERATE, and TROPICAL deforestation in both CESM1.0 and IPSL-CM5 models are analyzed and compared in section 3a. The results from the surface energy decomposition are discussed in section 3b (direct effects) and section 3c (indirect effects). The contributions of the two effects to teleconnection are discussed in section 3d.

Simulated surface temperature change

Conversion of forests to grasslands, in both CESM1.0 and IPSL-CM5, leads to substantially (above the plus or minus one standard deviation) large surface cooling in the northern high latitudes in all seasons in CESM1.0 and in most seasons in IPSL-CM5 for both the GLOBAL and BOREAL deforestation cases relative to the control (CTL) simulation (Fig. 2). In the GLOBAL case, the simulated boreal mean cooling varies from 4.62 to 6.46 K in CESM1.0 and from 0.94 to 1.69 K in IPSL-CM5 depending on the season (Table 1). When deforestation only occurs in the boreal region, the magnitude of boreal cooling is reduced in CESM1.0 (e.g., from 6.46 to 4.83 K in spring and from 4.62 to 3.53 K in fall; see Table 1). In contrast, IPSL-CM5 displays values of similar order of magnitude in the boreal region whether deforestation is global or limited only to high latitudes. Both global and boreal deforestation contribute to a global mean annual (as well as seasonal) cooling in CESM1.0 of 2.33 (2.04–2.64 K) and 1.53 K (1.40–1.85 K), respectively, and in IPSL-CM5 of 0.2 (0.04–0.24 K) and 0.54 K (0.42–0.61 K), respectively (Table 1).

Cooling in both models following deforestation results from the increased surface reflectivity (albedo) and consequent reduction of net solar radiation at the surface (Fig. S2 in the supplemental material) in high latitudes. Both CESM1.0 (Figs. S2b,c) and IPSL-CM5 (Figs. S2f,g) simulate a large reduction in net solar radiation during Northern Hemisphere (NH) spring and summer when solar insulation is maximum and correspondingly a strong cooling (Figs. 2b,c,f,g) in those two seasons in both models is simulated. In the two models, the cooler temperatures resulting from boreal deforestation are not restricted to boreal regions but rather extend to the temperate zone, albeit with smaller magnitude and significance (Fig. 2, cyan line).

Tropical deforestation results in tropical warming throughout the year, from approximately 0.11 to 0.19 K in CESM1.0 and from 0.94 to 1.29 K in IPSL-CM5 (Table 1 and Fig. 2). Although albedo is increased in those regions as in all deforested zones, the sum of turbulent heat transfer is reduced (Fig. S3 in the supplemental material). This change in turbulent heat fluxes dominates in the tropics and results in warming that overrides the albedo-induced cooling. The magnitude of

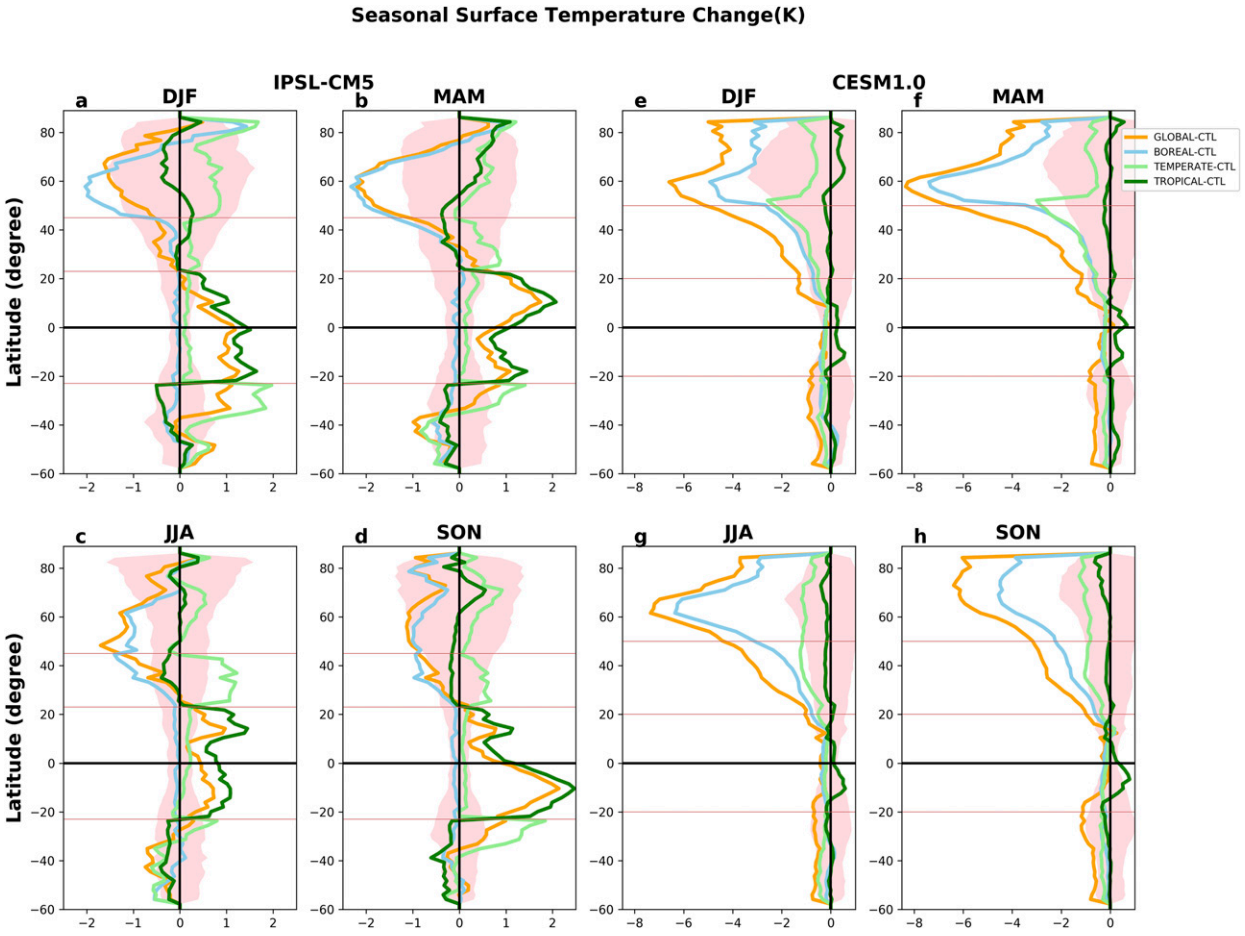

FIG. 2. Simulated changes in seasonal and zonal mean surface temperature between the deforestation experiments and the control simulation (a)–(d) over the last 30 years of 50-yr simulations in IPSL-CM5 and (e)–(h) over the last 50 years of 80-yr simulations in CESM1.0. Shading represents plus or minus one standard deviation from the respective model control simulations. Horizontal dashed lines show the various latitudinal bands where deforestation occurs in different experiments. Note that the *x*-axis scales differ between IPSL-CM5 and CESM1.0.

tropical mean warming simulated in CESM1.0 is quite smaller than IPSL-CM5 (approximately one-tenth) because the change in sensible heat flux is significantly larger ($\sim$12 W m^{-2}) when compared to other components of energy balance in IPSL-CM5; while this flux is almost unchanged in CESM1.0 ($\sim$1 W m^{-2}) (see Table S2 in the supplemental material; tropical means).

When changes in tropical surface temperature are diagnosed from the global deforestation simulation, the models do not agree on the sign of the simulated change. CESM1.0 indeed simulates a tropical mean cooling of 0.48–0.64 K whereas IPSL-CM5 still simulates a tropical mean warming but with reduced magnitudes (0.51–1.0 K) relative to the warming simulated in the tropical case (Table 1). Changes in the sign and magnitude of the tropical mean response for global deforestation in both models indicate that tropical regions are influenced by changes in temperate and/or boreal regions through atmospheric teleconnections.

Although there is consistency in the simulated temperature changes to boreal and tropical deforestation in the two models, their responses to temperate deforestation are opposite (Table 1 and Fig. 2). CESM1.0 simulates a systematic mean seasonal cooling in the temperate region (0.77–1.36 K; Table 1) with larger values during NH spring and winter (Figs. 2f,g), whereas IPSL-CM5 simulates warming varying from 0.24 K in winter to 0.9 K in summer (Table 1). In both models, net solar radiation is reduced in response to deforestation as is the sum of turbulent fluxes (Figs. S2 and S3). However, the change in turbulent fluxes is larger than the change in net shortwave radiation ΔSW_{net} in IPSL-CM5 while it is the reverse in CESM1.0. Hence CESM1.0 is more sensitive to albedo change resulting from

TABLE 1. Simulated global, regional, seasonal, and annual mean land surface temperature change (K) between deforestation and control experiments averaged over the last 50 years of 80-yr simulations for CESM1.0 and over last 30 years of 50-yr simulations for IPSL-CM5. Contrasting responses for temperate deforestation in the two models are highlighted with italics. Note that the means provided in this table are over entire latitudinal bands over land of their respective experiments, as described in section 2 (the methods section).

Experiments	CESM1.0					IPSL-CM5				
	DJF	MAM	JJA	SON	Annual	DJF	MAM	JJA	SON	Annual
Boreal mean change										
GLOBAL − CTL	−5.21	−6.46	−5.55	−4.62	−5.40	−1.21	−1.69	−1.09	−0.94	−1.23
BOREAL − CTL	−3.82	−4.83	−4.83	−3.53	−4.25	−1.49	−1.73	−0.81	−0.77	−1.2
Temperate mean change										
GLOBAL − CTL	−2.51	−2.89	−2.59	−2.25	−2.56	−0.37	−0.14	−0.43	−0.45	−0.35
TEMPERATE − CTL	*−1.04*	*−1.36*	*−0.93*	*−0.77*	*−1.02*	*0.24*	*0.51*	*0.90*	*0.45*	*0.52*
Tropical mean change										
GLOBAL − CTL	−0.64	−0.64	−0.55	−0.48	−0.57	0.70	1.00	0.50	0.92	0,78
TROPICAL − CTL	0.11	0.19	0.11	0.11	0.13	1.04	1.28	0.94	1.29	1.14
Global mean change										
GLOBAL − CTL	−2.38	−2.64	−2.45	−2.04	−2.33	−0.09	−0.10	−0.24	−0.04	−0.20
BOREAL − CTL	−1.51	−1.85	−1.77	−1.40	−1.53	−0.48	−0.61	−0.45	−0.42	−0.54
TEMPERATE − CTL	*−0.71*	*−0.80*	*−0.65*	*−0.56*	*−0.68*	*0.46*	*0.35*	*0.33*	*0.36*	*0.28*
TROPICAL − CTL	0.05	0.03	−0.06	−0.02	−0.01	0.35	0.45	0.28	0.44	0.40

deforestation than IPSL-CM5 (Table S2 and Figs. S2 and S3). Our results are consistent with Bonan (2008), who highlighted that, unlike boreal or tropical climate response to vegetation changes, temperate climate responses to temperate vegetation perturbation have more uncertainty and are less well understood. It is also in line with Davin and de Noblet-Ducoudré (2010) and Li et al. (2016), who showed that the albedo-induced cooling in the temperate regions competes with the turbulence-induced warming, with similar orders of magnitude. To sum up, the broader pattern of boreal cooling and tropical warming due to deforestation in our experiments agrees well with many previous observational and modeling investigations (Bala et al. 2007; Davin and de Noblet-Ducoudré 2010; Lee et al. 2011; Li et al. 2015, 2016) and hence we believe this pattern follows well-understood biophysical phenomena of land-cover change.

In contrast to inconsistent temperature change in response to temperate deforestation in the two models, global deforestation results in temperate mean cooling in both models and in all seasons (Fig. 2). This indicates the influence of boreal deforestation on the temperate region (another evidence of teleconnection). In CESM1.0, the cooling in the temperate region is amplified, whereas in IPSL-CM5 the cooling induced by boreal deforestation on temperate region more than offsets the warming and hence there is a net cooling in the temperate regions. Figure 3 illustrates the teleconnections that exist between a specific latitudinal band and the rest of the world. It shows the relationship between the surface temperature changes resulting from deforestation in the same region (x axis) to the surface temperature change resulting from global deforestation (y axis) for all seasons. In both models, the dominant influence on regional temperature change can be attributed to deforestation within that region. In CESM1.0, however, in all seasons, global deforestation results in cooling everywhere, amplifying regional cooling in temperate and boreal regions and overriding the small regional warming in the tropics. In IPSL-CM5 the teleconnection signals are smaller than those discussed in CESM1.0 for tropical and temperate regions and are very small for boreal regions, where regional changes are solely attributed to regional deforestation. This is visible in Fig. 3, where markers touch the linear 1:1 red line indicate weaker teleconnection signals.

b. *Net direct effect*

The net direct effect ΔTs_{direct} is estimated as the sum of the first three terms on the RHS of Eq. (3) and the spatial distribution is shown for all seasons in Figs. S4–S11 of the supplemental material. Here, we primarily focus on the boreal summer June–August (JJA) season, as on average there is a common robust signal in this season in both models when compared to other seasons (Table 1). The net direct effect causes warming in the two models over deforested locations (Figs. 4a,d,g,j and Figs. S4 and S8). The response to global deforestation, for example, warms the deforested global lands by approximately 0.08 K in CESM1.0 and by 0.94 K in IPSL-CM5 (Table 2 and Fig. 4a). The warming originates from decreased roughness length (and the consequent reduction in turbulent heat fluxes) following forest removal and is the dominant contribution in both models to the net direct change in surface temperature

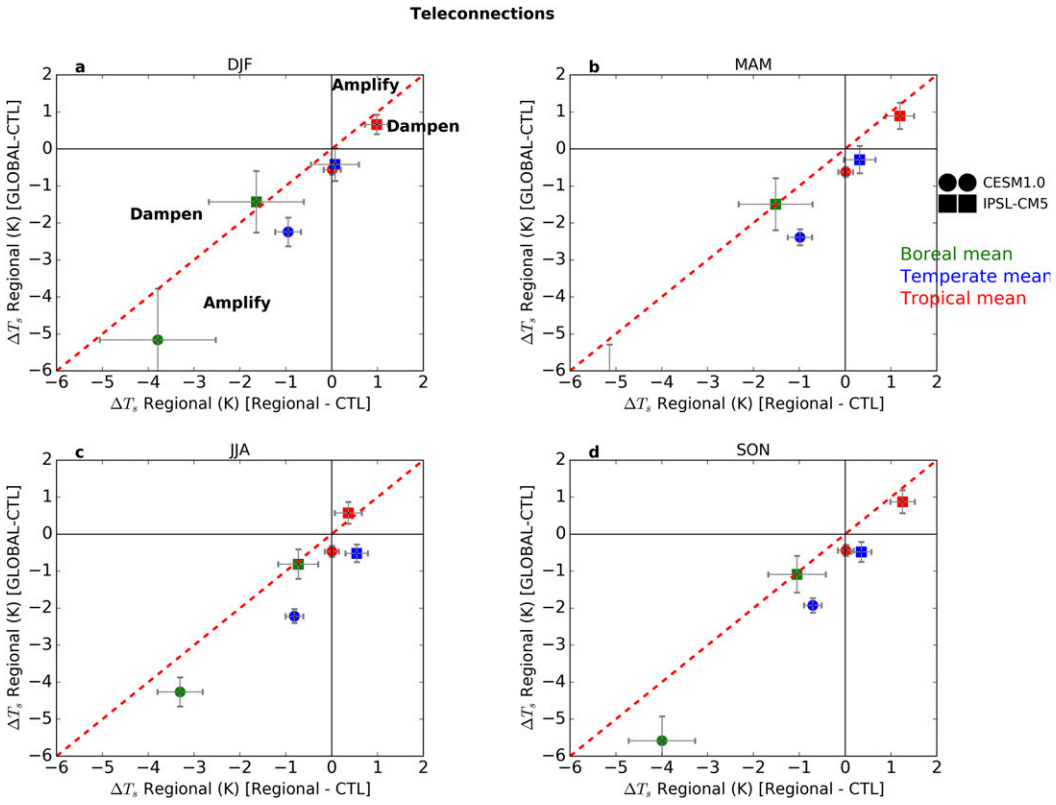

FIG. 3. Regional mean surface temperature changes in GLOBAL − CTL case against regional mean surface temperature changes in BOREAL − CTL (green markers), TEMPERATE − CTL (blue markers), and TROPICAL − CTL (red markers) cases for all the seasons in CESM1.0 (filled circles) and IPSL-CM5 (filled squares). The magnitude of interregional teleconnections can be estimated from the difference between the dashed red line and the markers for each region. Markers away from the red dashed line represent stronger interregional teleconnection effects (e.g., dots for CESM1.0), and markers that are closer to the dashed red line represent smaller interregional teleconnection effects (e.g., filled squares for IPSL-CM5). Error bars represent the standard error from the 50 seasonal mean differences in CESM1.0 simulations and 30 seasonal mean differences in IPSL-CM5 simulations.

(Fig. 4a). Indeed, increases in albedo tend to cool the deforested land, in both models (Fig. 4a) while changes in the Bowen ratio lead to very small warming in CESM1.0 and a negligible impact in IPSL-CM5. However, the effect of changes in roughness length is much larger in IPSL-CM5 and explains why this model has a much larger direct effect. Table S2 (see global means) indeed shows that the increase in r_a is about 10 times larger in IPSL-CM5 than in CESM1.0.

For the other seasons for this same simulation (GLOBAL; Table 2), the picture is quite similar: dominant impact of changes in roughness length that leads to warming in all seasons, and a systematic cooling impact due to changes in albedo. In IPSL-CM5, all regional deforestation experiments show changes similar to the GLOBAL experiment described above (Fig. 4). In CESM1.0, however, the response to changes in the Bowen ratio is warming for all regions, and in the case of boreal deforestation, the role of albedo is clearly larger than the role of changes in β. What is important to note is that the global mean temperature change due to direct effects are the smallest when compared to indirect effects (Table S2) in the global deforestation simulation in both models. In the cases of regional deforestation, direct effects are largest in the tropics and smallest in the boreal region (Table S2).

c. *Net indirect effect*

The net indirect effect $\Delta Ts_{indirect}$ resulting from deforestation is estimated by summing up the last three terms in the RHS of Eq. (3) and the spatial distribution for all four deforestation experiments are shown in Figs. S4–S7 (for IPSL-CM5) and Figs. S8–S11 (for CESM1.0) for all seasons. The net indirect effect causes mean cooling over deforested locations, boreal and temperate regions in CESM1.0 (Figs.4e,h), and boreal

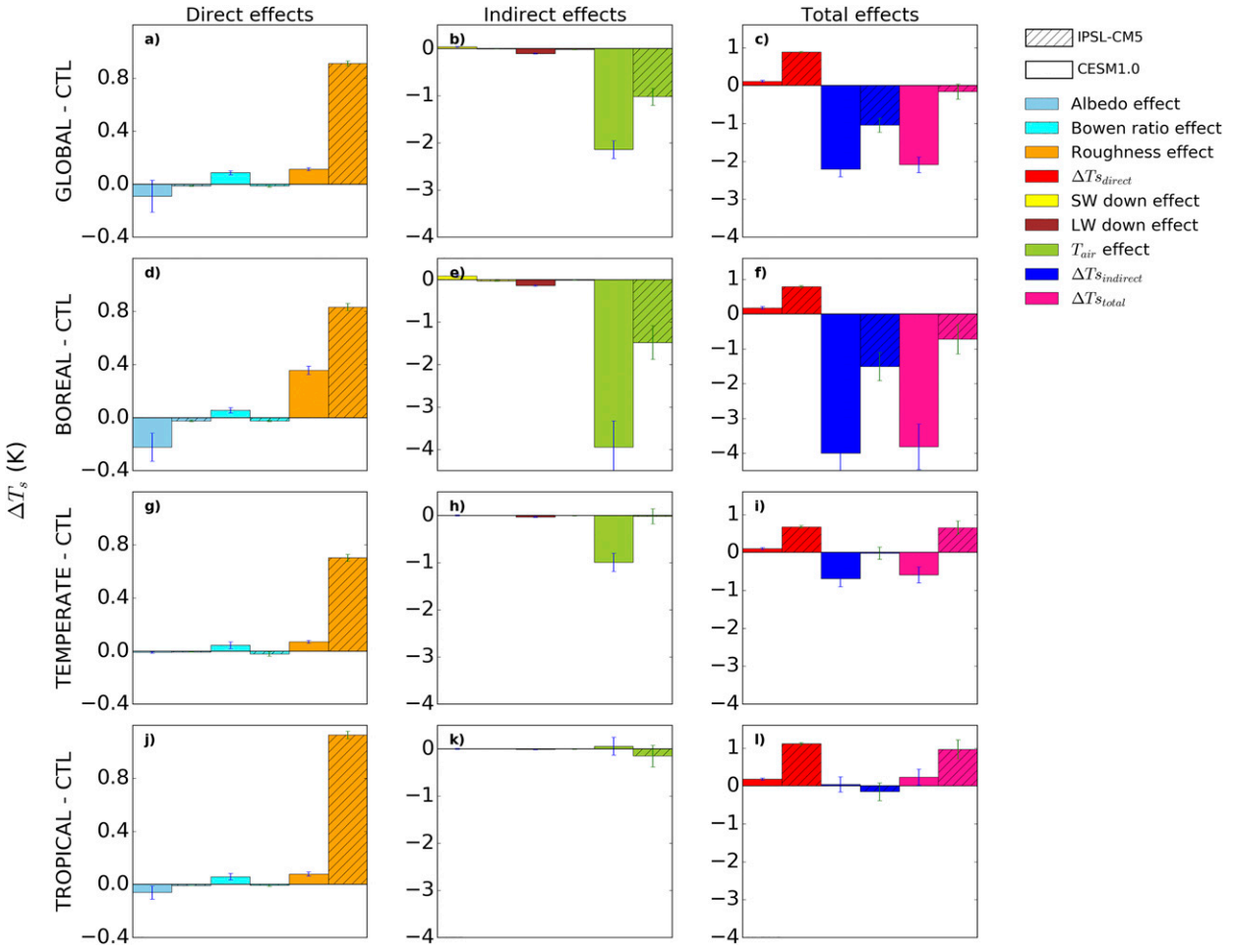

FIG. 4. Calculated deforestation-induced JJA mean surface temperature changes over deforested locations for the (a)–(c) GLOBAL, (d)–(f) BOREAL, (g)–(i) TEMPERATE, and (j)–(l) TROPICAL cases relative to the CTL case. CESM1.0 values are shown with plain bars while IPSL-CM5 bars are hatched. Error bars represent the standard error from the 50 seasonal mean differences in CESM1.0 and 30 seasonal means in IPSL-CM5. Note the difference in *y*-axis scales for the three columns.

and tropical regions in the IPSL-CM5 model (Figs. 4e,k). Small warming over the tropics in CESM1.0 (Fig. 4k), and over the temperate region in IPSL-CM5 is calculated (Fig. 4h). In the global deforestation, for example, indirect effects lead to global mean cooling over deforested locations in both models in all seasons (Table 2 and Fig. 4b). In particular, the summer mean cooling is 2.19 K in CESM1.0 and 1.17 K in IPSL-CM5 (Table 2). Two out of three indirect terms (downward longwave radiation and air temperature) contribute to this net cooling (Table 2 and Fig. 4b) and the other term (downward shortwave radiation) leads to a small warming. However, the magnitudes of warming are extremely small: 0.04 K for CESM1.0 and 0.01 K for IPSL-CM5. Downward longwave radiation at the surface decreases in both models, leading to cooling. Here again, values are very small and negligible with respect to the total indirect effect, −0.09 and −0.04 K for CESM1.0 and IPSL-CM5, respectively. Finally, the dominant contribution to indirect changes is the ambient air temperature that strongly decreases in both models and dominates the overall change in $\Delta Ts_{indirect}$, −2.14 and −1.14 K for CESM1.0 and IPSL-CM5, respectively.

Among the regional experiments, boreal deforestation induces the largest (−2.19 K; ~97%) and tropical region induces the smallest (0.06 K; ~40%) magnitudes of indirect effects in the CESM1.0 model (Table S2). The temperate region is a transition region and lies in between the two (−0.73 K). In IPSL-CM5, although the magnitude of temperate-deforestation-induced change in temperate region is smallest (−0.12 K compared to a tropical mean of −0.15 K and a boreal mean of −1.51 K), the percentage contribution of indirect effects to the total effect is smallest (~12%) in the tropics and largest in

TABLE 2. Calculated seasonal mean surface temperature change over deforested regions resulting from direct, indirect, and total effects in the GLOBAL deforestation experiment relative to the control simulation. For the first row of each season, the percentage change in parentheses for direct effects [computed as the ratio of absolute direct change to the sum of absolute direct and indirect effects, e.g., $|0.045|/(|0.045| + |-2.37|) \times 100 = 1.86\%$] and indirect effects (e.g., $100\% - 1.86\% = 98.14\%$). For the second row of each season, changes (K) in parentheses are, respectively, a result of albedo, roughness, and Bowen ratio changes under the direct effect column and a result of downwelling shortwave and longwave radiation and air temperature changes under the indirect effect column. Simulated changes are also given for the comparison with the calculated total effects. Changes are averaged over the last 50 years of 80-yr simulations for CESM1.0 and over the last 30 years of 50-yr simulations for IPSL-CM5. The rows in italics are often used in the text to discuss and highlight the results. Interannual variability is assessed from the control experiment in their respective model simulations. Interannual variability is the standard deviation calculated using 30-yr seasonal means in IPSL-CM5 and 50-yr seasonal means in CESM1.0.

		Change in global mean land surface temperature (K)				
Model	Seasons	Direct effect ($\Delta\alpha$, Δr_a, $\Delta\beta$)	Indirect effect (ΔSW_{inc}, ΔLW_{inc}, ΔT_a)	Total effect	Simulated effect	Interannual variability (K)
CESM1.0	DJF	0.045 (1.86) (−0.04, 0.06, 0.025)	−2.37 (98.14) (0.02, −0.25, −2.14)	−2.32	−2.38	±0.25
	MAM	0.097 (3.62) (−0.022, 0.133, 0.014)	−2.58 (96.38) (0.008, −0.064, −2.52)	−2.48	−2.64	±0.20
	JJA	*0.08 (2.7)* *(−0.06, 0.08, 0.06)*	*−2.19 (97.3)* *(0.04, −0.09, −2.14)*	*−2.11*	*−2.16*	*±0.19*
	SON	0.063 (2.9) (−0.017, 0.14, 0.06)	−2.05 (97.1) (0.01, −0.090, −1.97)	−1.99	−2.04	±0.15
IPSL-CM5	DJF	0.34 (44.2) (−0.11, 0.35, −0.10)	−0.43 (55.8) (0.01, −0.11, −0.33)	−0.09	−0.08	±0.02
	MAM	0.72 (47.4) (−0.01, 0.75, −0.02)	−0.80 (52.6) (0.000, −0.04, −0.76)	−0.08	−0.1	±0.01
	JJA	*0.94 (44.55)* *(−0.013, 0.97, −0.015)*	*−1.17 (55.45)* *(0.01, −0.04, −1.14)*	*−0.23*	*−0.24*	*±0.02*
	SON	0.59 (47.9) (−0.005, 0.64, −0.04)	−0.64 (52.1) (0.002, −0.008, −0.63)	−0.05	−0.04	±0.01

boreal regions (~66%; Table S2). In summary, we find that the net indirect effect is dominated by changes in ambient air temperature in both the models in all the regions and seasons, while the contributions from other feedback terms (downwelling shortwave and longwave radiation) are relatively smaller. We infer that the dominance of indirect air temperature feedback is likely due to two effects (Table S2): 1) reduced sensible heat flux and therefore reduced warming of the air by land, and 2) decreased incoming radiations resulting from land-induced changes in water vapor and cloudiness.

d. *Contribution of direct and indirect effects to teleconnection*

Figure 5 shows the zonal changes in direct, indirect, and total surface temperature for all four simulations and for both models. As expected, direct temperature changes are confined mostly to deforested locations in the two models, while the influence of indirect effects can be seen away from the deforested locations and are solely responsible for temperature changes in remote locations (e.g., see Figs. 5b,f and Figs. S4–S11). IPSL-CM5 exhibits clear and strong direct changes, whereas changes are very small for CESM1.0 over deforested locations. Therefore in both the models, direct effects of regional deforestations do not affect the regions away from the deforested locations and hence their contribution to teleconnections is small.

Figure 6 shows the magnitude of teleconnections calculated as the changes in surface temperature triggered in a latitudinal band by the area deforested in another latitudinal band. Whatever the region, there is a relatively large intermodel dispersion, CESM1.0 model triggering larger teleconnections than IPSL-CM5. In both models tropical deforestation does not affect boreal regions, while the tropics are affected by both temperate and boreal deforestation albeit the changes are small (<0.4°C). Boreal and temperate regions strongly affect one another; the boreal region teleconnection influence is 25% larger than that of temperate region teleconnection. This result demonstrates that forests removal in the northern high latitudes, for example, results in less solar radiation absorption (Fig. S2), which leads to cooling at the surface and is further amplified indirectly by air temperature feedback (Fig. 4). This larger indirect effect in the northern high latitudes extends the cooling into the tropics in both the models (Fig. 5), triggering teleconnections: an energy imbalance

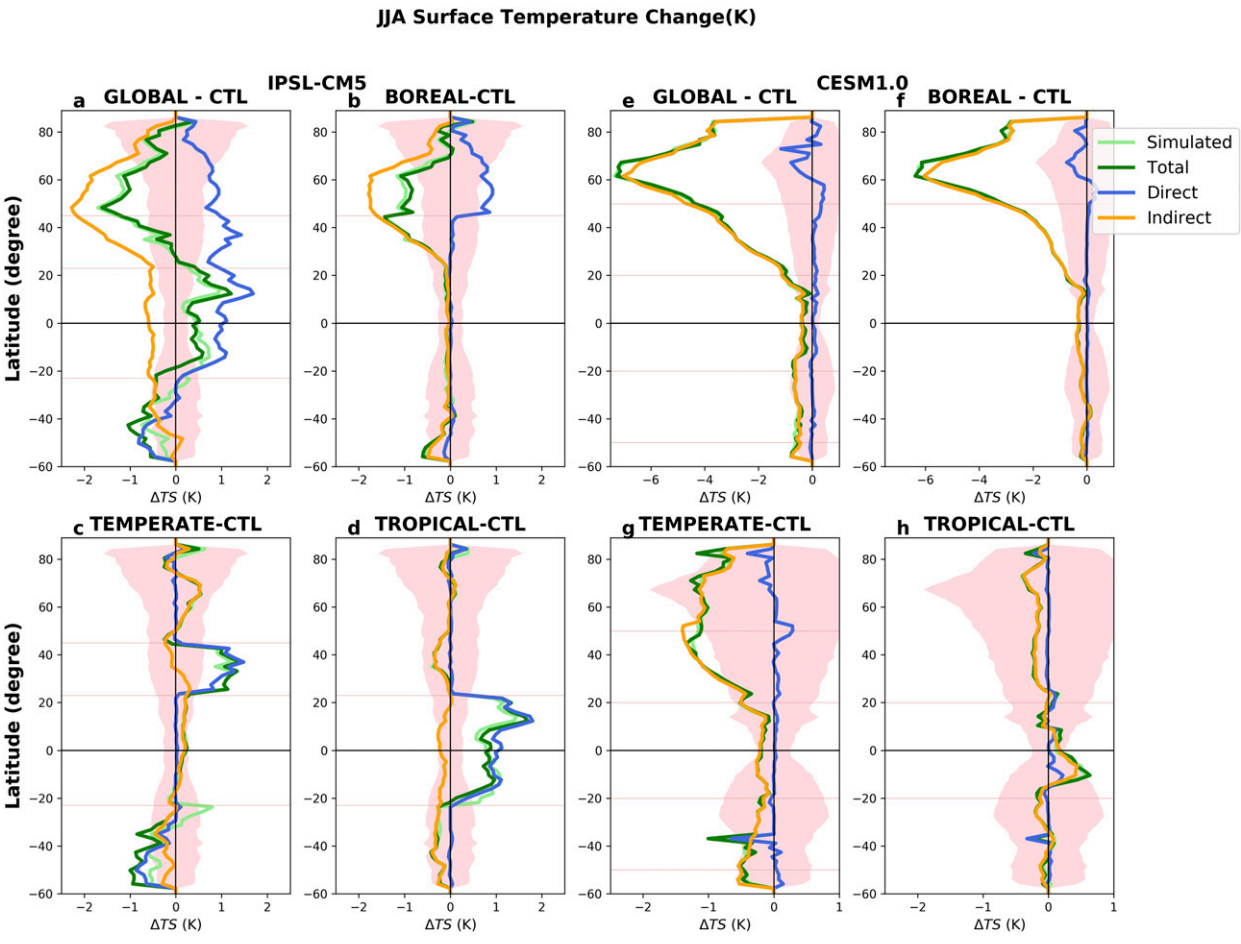

FIG. 5. Zonal mean and JJA mean changes in land surface temperature (K) due to direct, indirect, total effects (sum of direct and indirect effects), and simulated change (from model output) in the GLOBAL, BOREAL, TEMPERATE, and TROPICAL deforestation experiments relative to CTL simulation. Shading represents plus or minus one standard deviation from the respective model control simulations.

between hemispheres is created that causes shifts in atmospheric circulation [the circulation changes are described in more detail in Devaraju et al. (2015) and Laguë and Swann (2016)].

e. *Realistic historical and future LULCC simulation results*

Using Eq. (3) we estimate the various contributions to changes in surface temperature for 1) the historical LULCC relative to preindustrial vegetation (comparing 1992 vegetation to that of 1870) and 2) the future LULCC relative to the present day. These analyses are made using the simulations from LUCID project.

1) EFFECTS OF HISTORICAL LULCC

Table 3 provides the quantified numbers of direct, indirect, and total effects for each model for the boreal summer season. Most of the changes in land use during the historical period occurred in the temperate regions (see Fig. 1 of Boisier et al. 2012) and hence the means given in Table 3 are restricted to only those regions where deforestation occurs. Four out of seven models [ARPEGE, Conformal–Cubic Atmospheric Model (CCAM), Community Climate System Model (CCSM), and ECHAM5] show warming as a result of direct effects and cooling as a result of indirect effects (Table 3). This is consistent with the idealized simulation results shown for CESM1.0 above. Two models [EC-EARTH and the Simplified Parameterizations, Primitive-Equation Dynamics (SPEEDY) model] simulate systematic cooling in response to both direct and indirect effects of historical deforestation. IPSL-CM5 results are consistent with the idealized temperate deforestation (i.e., exhibiting warming from direct and indirect effects). In five out of seven models (ARPEGE, CCAM, CCSM, EC-EARTH, and ECHAM5), the indirect

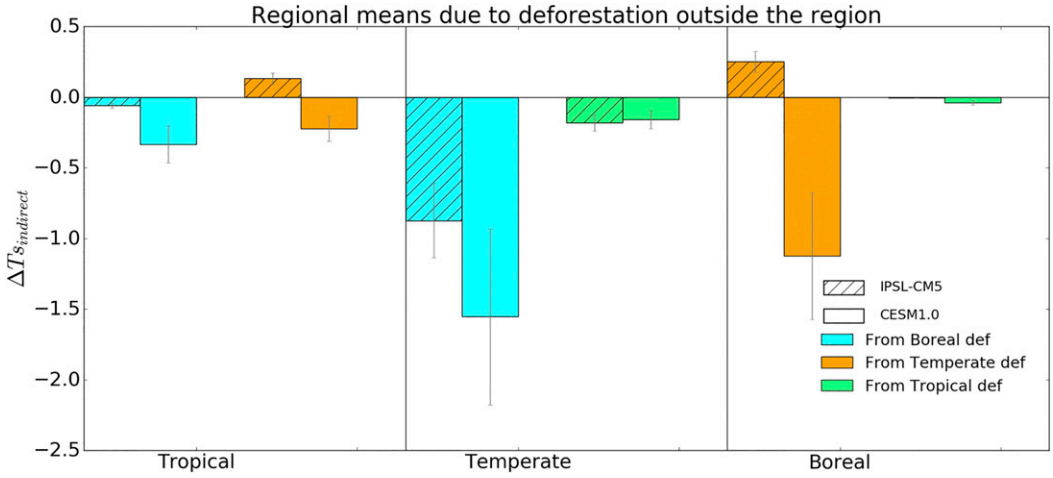

FIG. 6. Regional mean JJA surface temperature changes from indirect effects due to deforestation outside the region. The mean changes in each region provide the magnitude of teleconnections from one region to the other regions. CESM1.0 values are shown with plain bars while the bars for IPSL-CM5 are hatched. Error bars represent the standard error from the 50 seasonal mean differences in CESM1.0 and 30 seasonal means in IPSL-CM5. Colors (cyan, orange, and light green) distinguish the contribution of indirect effects from boreal, temperate, and tropical deforestation.

contribution to the total change in surface temperature is the dominant signal (Table 3 and Fig. S12 in the supplemental material), as in the CESM1.0 idealized simulations. In the two remaining models (IPSL-CM5 and SPEEDY), the direct effect contribution to the total change in surface temperature is the largest, as in the IPSL-CM5 idealized simulations. The major contribution of air temperature to indirect effects is found in all models, as is the major contribution of roughness length to direct effects (Fig. S12). Overall, the atmospheric feedbacks or indirect effects in the temperate regions are solely responsible for the historical surface cooling, and nearly 70% of the models agree.

2) EFFECTS OF FUTURE LULCC

Most of the projected deforestation under the RCP8.5 scenario occurs in the tropical regions in all of the LUCID-CMIP5 models used here. However, afforestation takes place in parts of temperate and boreal regions (Fig. 1 of Brovkin et al. 2013; Quesada et al. 2017). Hence we only extract the means over deforested tropical regions and compare with idealized tropical simulations. All four models show net warming in response to tropical deforestation in the future. This is dominated by warming due to direct effects in almost all of the models (Table 3). Only CanESM2 shows a smaller direct effect (~28%) than indirect effect (~72%). Furthermore, only IPSL-CM5-LR shows small cooling due to indirect effects. The HadGEM2-ES has a similar order of magnitudes for both direct and indirect effects. Again in these LUCID-CMIP5 models, a change in roughness length is the main contributor to direct effects, while a change in air temperature is the main contributor to indirect effects. In summary, the realistic future LULCC simulation results confirm the idealized simulation results of tropical deforestation. Therefore, in the future, a net warming over the tropics due to tropical deforestation is projected to be driven mostly by direct effects (~50%–90%) in three LUCID-CMIP5 models and relatively smaller contribution from indirect effects (~9%–50%) (Table 3 and Fig S13 in the supplemental material).

4. Discussion and conclusions

In this study, we investigated the relative importance of direct and indirect biophysical effects of LULCC on land surface temperature. We used various climate model simulations (two models with four idealized simulations, seven models with two historical simulations, and four models with two future scenario simulations, for a total of ~30 simulations) with idealized and realistic (observed and scenario) changes in vegetation distribution. Most of the deforestation simulations (in both idealized and realistic historical LULCC) show larger changes in surface temperature through indirect effects: changes due to indirect effects are at least as large as, and often larger than, direct effects in the northern middle and high latitudes (Figs. 7 and S12). This highlights the importance of indirect effects from the atmospheric feedback for offline prediagnoses of future LULCC. In contrast, tropical deforestation (in both idealized and

TABLE 3. Changes in JJA mean surface temperature over deforested grid cells resulting from direct, indirect, and total effects for LUCID (temperate mean: 23°–45°N) and LUCID-CMIP5 (tropical mean: 23°S–23°N) simulations. For the first row of each model, percentage change in parentheses for direct effects [computed as the ratio of absolute direct change to sum of absolute direct and indirect changes, e.g., $|0.005|/(|0.005| + |-0.325|) \times 100 = 1.51\%$] and indirect effects (e.g., $100\% - 1.51\% = 98.49\%$). For the second row of each model, Changes (K) in parentheses are, respectively, a result of albedo, roughness and Bowen ratio changes under the direct effect column and a result of downwelling shortwave and longwave radiation and air temperature changes under the indirect effect column. Simulated changes are also given for comparison with total effect. (Expansions of acronyms are available online at http://www.ametsoc.org/PubsAcronymList.)

		Surface temperature change (K)			
LULCC forcing	Model	Direct effect ($\Delta\alpha$, Δr_a, $\Delta\beta$)	Indirect effect (ΔSW_{inc}, ΔLW_{inc}, ΔT_a)	Total effect	Simulated changes
Past (1992 vegetation relative to 1870 vegetation)	ARPEGE	0.005 (1.51) (−0.010, 0.020, −0.005)	−0.325 (98.49) (0.001, −0.003, −0.323)	−0.320	−0.334
	CCAM	0.009 (3.14) (0.002, 0.075, −0.067)	−0.277 (96.86) (−0.001, −0.022, −0.254)	−0.268	−0.198
	CCSM	0.106 (49.30) (−0.003, 0.122, −0.013)	−0.109 (50.70) (−0.002, −0.008, −0.099)	−0.003	−0.002
	EC-EARTH	−0.026 (5.09) (−0.030, 0.078, −0.074)	−0.484 (94.91) (−0.006, −0.015, −0.463)	−0.510	−0.454
	ECHAM5	0.010 (6.76) (−0.001, 0.014, −0.003)	−0.138 (93.24) (−0.001, −0.001, −0.136)	−0.128	−0.128
	IPSL-CM5	0.046 (75.41) (−0.002, 0.042, 0.006)	0.015 (24.59) (0.001, −0.002, 0.016)	0.061	0.057
	SPEEDY	−0.143 (80.79) (−0.041, −0.163, 0.061)	−0.034 (19.21) (0.027, −0.007, −0.054)	−0.177	−0.219
Future (RCP8.5 − L2A85)	CanESM2	0.031 (28.18) (−0.001, 0.016, 0.016)	0.079 (71.82) (0.001, 0.001, 0.077)	0.110	0.101
	IPSL-CM5A-LR	0.092 (81.42) (−0.001, 0.090, 0.003)	−0.021 (18.58) (−0.001, 0.003, −0.022)	0.071	0.060
	MPI-ESM-LR	0.399 (90.88) (−0.003, 0.379, 0.023)	0.040 (9.12) (0.001, 0.000, 0.039)	0.439	0.302
	HadGEM2-ES	0.156 (50.16) (−0.006, 0.068, 0.094)	0.155 (49.84) (0.010, −0.011, 0.156)	0.311	0.321

realistic future LULCC) simulations show larger direct effects compared to indirect effects (Figs. 7 and S13). However, we find a considerable spread among multiple models (Figs. S12 and S13) in partitioning between direct and indirect effects which may explain part of the intermodel spread found in previous studies that compare the total biophysical effects across models (de Noblet Ducoudré et al. 2012).

In the idealized regional deforestation simulations, boreal regions experience the largest cooling from indirect effects and tropics experience the largest warming from direct effects in both the NCAR CESM1.0 and IPSL-CM5 (Table S2 and Fig. 7). The predominance of cooling due to indirect effect is also confirmed by the realistic historical LULCC simulations in most of the LUCID models and in most of the seasons in the temperate region (Table 3 and Fig. S12). In the future LULCC simulations, the response of tropical region also confirms the dominance of warming from direct effects (Table 3 and Fig. S13). The cooling from indirect effects is largely due to changes in air temperature feedback and the warming from direct effects in the tropics is largely due to roughness length change. The partitioning of indirect effects in this study reveals that the change in air temperature dominates the other two indirect effects (downward shortwave and longwave radiation changes). CD16 did not separate these two indirect effects.

Furthermore, our idealized deforestation simulations show teleconnections in both the models. Among direct and indirect effects, we found that direct effects are mostly associated with local changes (effects larger over deforested regions) whereas indirect effects contribute to both local and remote changes (effects larger over and beyond the deforested regions, Fig. 5). The magnitude of teleconnections estimated for each region (tropics, temperate, and boreal regions) are shown in Fig. 6 for the two models. A boreal deforestation teleconnection effect on the temperate region is largest in magnitude in CESM1.0, and a temperate deforestation teleconnection effect on the boreal region is largest in IPSL-CM5. Tropical deforestation affects only the immediate neighboring temperate region in the two models. These results highlight the importance of teleconnections from indirect effects. Hence we infer that

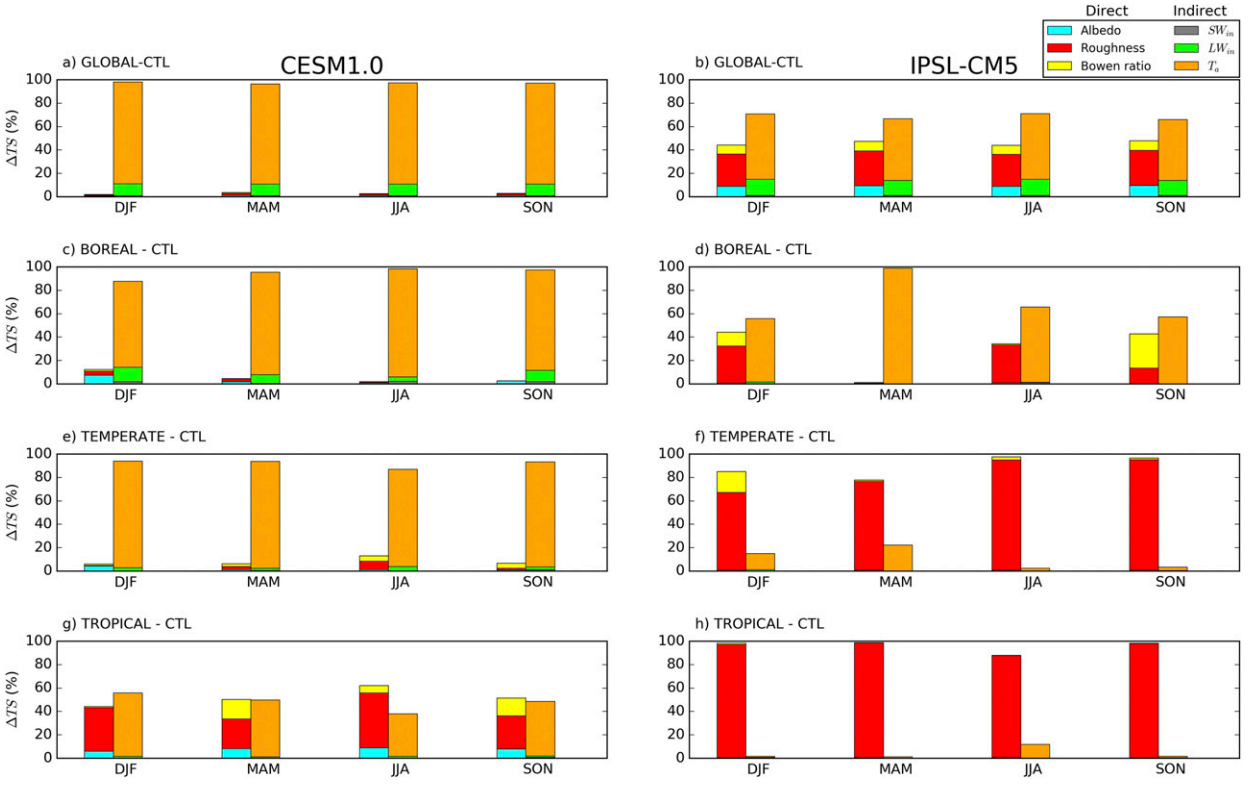

FIG. 7. Contribution of direct and indirect effects to total change in surface temperature over deforested regions in all seasons and for all deforestation experiments in (a),(c),(e),(g) CESM1.0 and (b),(d),(f),(h) IPSL-CM5. The first set of colors (cyan, red, and yellow) is contributions from albedo change, roughness change and Bowen ratio change to direct effects (%), and the second set of colors (gray, green, and orange) is contributions from downwelling shortwave and longwave radiation and air temperature change to indirect effects (%).

the results from offline land surface model simulations that do not account for atmospheric feedbacks and eventually teleconnections could underestimate or even simulate an opposite sign of climate change depending on the location of LULCC.

For global deforestation scenarios (e.g., global forests replaced by grasslands), the contribution of direct effect to global mean warming is smaller, 2%–4% in CESM1.0 and 44%–48% in IPSL-CM5 different in seasons (Fig. 7 and Table 2), but the contribution of indirect effect to cooling is larger (96%–98% in CESM1.0 and 52%–56% in IPSL-CM5; Fig. 7). Hence, for instance, the net impact of direct and indirect effects is a global mean cooling of 2.11 and 0.23 K, respectively, in JJA (Table 2). The total cooling calculated from Eq. (3) closely matches the simulated global mean cooling of 2.16 and 0.24 K in the two models, respectively (Table 2).

Our analysis shows that the LULCC between present-day (1992) and preindustrial period (1870) caused cooling in most of the models mainly as a result of indirect effects (>90% of total change; Fig. S12) and slight warming as a result of direct effects (<10% of total change). Most of the historical deforestation took place in northern temperate regions, where indirect effects dominate. Most of the future deforestation is projected over the tropics, where direct effects dominate: in the future, warming due to direct effects of projected LULCC (>50% of total change) dominates indirect effects (<50% of total change; Fig. S13).

On average there is good agreement between CESM1.0 and IPSL-CM5 in the sign of change (in both direct and indirect effects) resulting from large-scale idealized deforestation. However, there is still a large difference in the magnitude of the response between the two models. Even though the area of boreal deforestation in CESM1.0 ($\sim 14 \times 10^6\,\mathrm{km}^2$) is smaller compared to IPSL-CM5 ($\sim 23 \times 10^6\,\mathrm{km}^2$), CESM1.0 simulates a larger snow cover change in the boreal region (Table S2) and hence a strong correlation between air and surface temperature change (Fig. 8a; correlation 0.99, with $p < 0.005$); IPSL-CM5 simulates smaller changes in snow cover and also does not exhibit such a strong correlation (0.45; $p < 0.005$), hence the cooling is smaller in this model. In the tropics, there is a strong

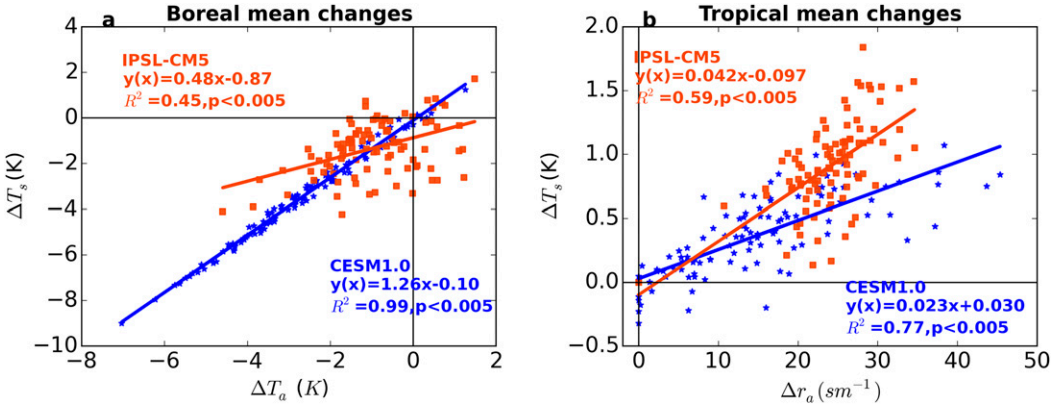

FIG. 8. (a) Changes in boreal mean surface temperature (K) against changes in boreal mean air temperature (K) for GLOBAL − CTL case [term VI in Eq. (3)]. (b) Changes in tropical mean surface temperature against changes in tropical mean aerodynamic resistance for TROPICAL − CTL case [term III in Eq. (3)]. Lines are the linear regression fits for the two models [CESM1.0 (blue) and IPSL-CM5 (orange)] from the first 96 months of the simulations (temporal trend within first 8 yr; monthly data are used to have more data points for the regression; and the simulations start equilibrating from the 8th year). Note that (a) represents the relationship between surface temperature and air temperature in the boreal region (dominating indirect effects) and (b) represents the relationship between surface temperature and aerodynamic resistance in the tropical region (dominating direct effects).

correlation between changes in surface temperature and aerodynamic resistance (because of roughness length change) in both models (Fig. 8b; correlation 0.59 in IPSL-CM5 and 0.77 in CESM1.0, with $p < 0.005$) but the sensitivity is larger in the IPSL-CM5 model. CESM1.0 is nearly 3 times more sensitive (slope 1.26 K K^{-1}) to changes in air temperature than IPSL-CM5 (slope 0.48 K K^{-1}) in the boreal region, whereas in the tropics, IPSL-CM5 is two times more sensitive [slope 0.042 K (s m^{-1})$^{-1}$] to changes in aerodynamic resistance compared to CESM1.0 [slope 0.023K (s m^{-1})$^{-1}$]. This indicates that the partitioning of direct and indirect effect differs substantially between the models both in idealized and realistic simulations. Hence, there is a need for more model intercomparison exercises that will help to better understand the individual processes and improve the models.

The differences in the climate responses of the models to similar forest removal across the latitudinal bands can also be understood just through the ΔSW_{net} and latent heat flux change ΔLE components of the surface energy balance as reported by Li et al. (2016) using an intermediate complexity model. However, this claim by Li et al. is not always true in a complex model like IPSL-CM5. As shown in Fig. S14 of the supplemental material for IPSL-CM5, we find that ΔH is also required along with ΔSW_{net} and ΔLE (left y axis) to determine the sign and magnitude of ΔT_s (right y axis). For instance, IPSL-CM5 simulates an almost similar decrease in both ΔLE and ΔSW_{net} but a larger decrease in sensible heat flux change ΔH, and hence a larger warming due to direct effects that are dominated by roughness length changes through ΔH (Fig. 4j). In CESM1.0 over the tropics (Fig. S15 in the supplemental material), the decrease in ΔLE (warming effect) is larger than the decrease in ΔSW_{net} (cooling effect), and hence a warming is simulated as a result of tropical deforestation (Fig. 4l). However, in the boreal region, both IPSL-CM5 and CESM1.0 simulate a larger decrease in ΔSW_{net} than ΔLE (Figs. S14 and 15), leading to large cooling in the northern high latitudes dominated by air temperature feedback (Fig. 4e). The temperate region is a transition zone and thus the effects ofΔSW_{net} and ΔLE are close to each other, leading to uncertainty in the sign of change in surface temperature in the two models (Figs. S14 and 15).

The decomposition method does have some limitations because Eq. (3) does not account for the complete nonlinear interactions between each of its terms. For example, Bowen ratio changes are driven by both sensible and latent heat flux changes through circulation changes, humidity changes, and so on. Aerodynamic resistance changes are driven by air temperature and sensible heat flux changes, which might partly influence direct effects. A recent study by Rigden and Li (2017) shows that the partitioning between aerodynamic resistance and Bowen ratio terms can be substantially influenced by their interactions (although their sum is not influenced). In particular, the contribution of aerodynamic resistance may be overestimated (and thus the role of Bowen ratio underestimated) by assuming independence between the aerodynamic resistance and

the Bowen ratio. However, the higher-order interactions between direct and indirect effects are likely to be much smaller and hence are neglected here. The comparison of total effects calculated with the simulated effects (Fig. 5) reveals that the higher-order interactions are indeed negligible in this study and hence our conclusions are not affected by omitting them. The comparison of idealized and realistic simulations is also limited in usefulness because the simulations are not from the same versions of the models. It would have been very useful to investigate the role of background climates on the magnitude of direct and indirect effects if both idealized and realistic LULCC simulations were from the same model versions. The newly planned CMIP6-Land Use Model Intercomparison Project (LUMIP) exercise (Lawrence et al. 2016) will serve this purpose. Nevertheless, the conceptual decomposition of direct from indirect effects in this study helps improve our understanding of the biophysical effects of deforestation.

SSTs in historical LULCC simulations are fixed; if they were dynamic, then ocean feedbacks might also contribute to indirect effects as reported by Davin and de Noblet-Ducoudré (2010), and the magnitude of indirect effects for historical LULCC might change. The higher climate variability of indirect effects in the extratropics may not affect our conclusions from the past and future LUCID simulations (Figs. S12 and S13; error bars are smaller). The different latitudinal band cutoffs for the deforested regions between IPSL-CM5 and CESM1.0 do not affect our comparison because there is a negligible difference in surface temperature changes (Table S1) over deforested grid cells for different delimitations in the two models. Further, the direct and indirect effects calculations shown in Fig. 4 are reproduced in Fig.S16 of the supplemental material for the minimum shared deforested band cutoffs in the two models. We find no difference between Fig. 4 and Fig. S16 (specifically Figs. 4d–l and Figs. S16d–l), so we are confident that the difference in cutoffs of deforested regions does not affect our conclusions. We caution that our results [as well as those of CD16 and Bright et al. (2017)] might be influenced by nonlinear parameter interactions if daytime and nighttime values are considered separately (e.g., Lee et al. 2011).

In summary, our results highlight that the indirect feedback effects from changes in atmospheric conditions due to LULCC have important implications for studies that do not consider them (Alkama and Cescatti 2016; Duveiller et al. 2018). Usually, offline modeling studies assess the climate change impacts by assuming small indirect feedback effects (Schimel et al. 2015; Piao et al. 2013; Fisher et al. 2013; Murray-Tortarolo et al. 2013; Gerber et al. 2013). This assumption ignores the importance of indirect effects. Therefore, we emphasize that the inclusion of indirect feedback effect will improve the quantitative estimates of climatic changes resulting from large-scale land cover changes. Furthermore, along with the integrated indirect feedback effects, it is important to estimate individual conventional feedback effects such as water vapor, lapse rate, cloud, and soil moisture feedbacks as highlighted by many previous studies (Bala et al. 2007; Bonan 2008; Pielke et al. 2011; CD16). These individual feedback effects in the context of large-scale land cover changes need further attention in the future.

Acknowledgments. This work is performed in the framework of the European Commission FP7 LUC4C project (http://luc4c.eu; Grant 603542). The Community Earth System Model used for these simulations is publicly available online from the National Center for Atmospheric Research (CAM5.0 atmospheric model: http://www.cesm.ucar.edu/models/cesm1.0/cam/docs/ug5_0/ug.html and CLM4: http://www.cesm.ucar.edu/models/cesm1.0/clm/models/lnd/clm/doc/UsersGuide/book1.html). The IPSL-CM5 model is also available upon request (http://forge.ipsl.jussieu.fr/igcmg/wiki/IPSLCMIP5). We thank the data producers from the LUCID and LUCID-CMIP5 projects (https://www.mpimet.mpg.de/en/science/the-land-in-the-earth-system/working-groups/climate-biogeosphere-interaction/lucid-cmip5/experiments/): Vivek Arora, Juan Pablo Boisier, Victor Brovkin, Patricia Cadule, Veronika Gayler, Etsushi Kato, Andy Pitman, Julia Pongratz, and Eddy Robertson, for producing and making available their model output and for their contribution.

REFERENCES

Alkama, R., and A. Cescatti, 2016: Biophysical climate impacts of recent changes in global forest cover. *Science*, **351**, 600–604, https://doi.org/10.1126/science.aac8083.

Bala, G., K. Caldeira, M. Wickett, T. J. Phillips, D. B. Lobell, C. Delire, and A. Mirin, 2007: Combined climate and carbon-cycle effects of large-scale deforestation. *Proc. Natl. Acad. Sci. USA*, **104**, 6550–6555, https://doi.org/10.1073/pnas.0608998104.

Baldocchi, D., and S. Ma, 2013: How will land use affect air temperature in the surface boundary layer? Lessons learned from a comparative study on the energy balance of an oak savanna and annual grassland in California, USA. *Tellus*, **65B**, 19994, https://doi.org/10.3402/tellusb.v65i0.19994.

Barr, A. G., and A. K. Betts, 1997: Radiosonde boundary layer budgets above a boreal forest. *J. Geophys. Res.*, **102**, 29 205–29 212, https://doi.org/10.1029/97JD01105.

Bathiany, S., M. Claussen, V. Brovkin, T. Raddatz, and V. Gayler, 2010: Combined biogeophysical and biogeochemical effects of large-scale forest cover changes in the MPI Earth system

model. *Biogeosciences*, **7**, 1383–1399, https://doi.org/10.5194/bg-7-1383-2010.

Betts, R. A., 2001: Biogeophysical impacts of land use on present-day climate: Near-surface temperature and radiative forcing. *Atmos. Sci. Lett.*, **1**, 39–51, https://doi.org/10.1006/asle.2001.0023.

——, and Coauthors, 2007: Projected increase in continental runoff due to plant responses to increasing carbon dioxide. *Nature*, **448**, 1037–1042, https://doi.org/10.1038/nature06045.

Boisier, J. P., and Coauthors, 2012: Attributing the impacts of land-cover changes in temperate regions on surface temperature and heat fluxes to specific causes: Results from the first LUCID set of simulations. *J. Geophys. Res.*, **117**, D12116, https://doi.org/10.1029/2011JD017106.

Bonan, G. B., 2002: *Ecological Climatology: Concepts and Applications.* 2nd ed. Cambridge University Press, 550 pp.

——, 2008: Forests and climate change: Forcings, feedbacks, and the climate benefits of forests. *Science*, **320**, 1444–1449, https://doi.org/10.1126/science.1155121.

Bright, R. M., K. Zhao, R. B. Jackson, and F. Cherubini, 2015: Quantifying surface albedo and other direct biogeophysical climate forcings of forestry activities. *Global Change Biol.*, **21**, 3246–3266, https://doi.org/10.1111/gcb.12951.

——, E. Davin, T. O'Halloran, J. Pongratz, K. Zhao, and A. Cescatti, 2017: Local temperature response to land cover and management change driven by non-radiative processes. *Nat. Climate Change*, **7**, 296–302, https://doi.org/10.1038/nclimate3250.

Brovkin, V., and Coauthors, 2013: Effect of anthropogenic land-use and land-cover changes on climate and land carbon storage in CMIP5 projections for the twenty-first century. *J. Climate*, **26**, 6859–6881, https://doi.org/10.1175/JCLI-D-12-00623.1.

Chen, L., and P. A. Dirmeyer, 2016: Adapting observationally based metrics of biogeophysical feedbacks from land cover/land use change to climate modeling. *Environ. Res. Lett.*, **11**, 034002, https://doi.org/10.1088/1748-9326/11/3/034002.

Davin, E. L., and N. de Noblet-Ducoudré, 2010: Climatic impact of global- scale deforestation: Radiative versus nonradiative processes. *J. Climate*, **23**, 97–112, https://doi.org/10.1175/2009JCLI3102.1.

de Noblet-Ducoudré, N., and Coauthors, 2012: Determining robust impacts of land-use-induced land cover changes on surface climate over North America and Eurasia: Results from the first set of LUCID experiments. *J. Climate*, **25**, 3261–3281, https://doi.org/10.1175/JCLI-D-11-00338.1.

Devaraju, N., G. Bala, and A. Modak, 2015: Effects of large-scale deforestation on precipitation in the monsoon regions: Remote versus local effects. *Proc. Natl. Acad. Sci. USA*, **112**, 3257–3262, https://doi.org/10.1073/pnas.1423439112.

Dufresne, J. L., and Coauthors, 2013: Climate change projections using the IPSL-CM5 Earth System Model: From CMIP3 to CMIP5. *Climate Dyn.*, **40**, 2123–2165, https://doi.org/10.1007/s00382-012-1636-1.

Duveiller, G., J. Hooker, and A. Cescatti, 2018: The mark of vegetation change on Earth's surface energy balance. *Nat. Commun.*, **9**, 679, https://doi.org/10.1038/s41467-017-02810-8.

Fisher, J. B., and Coauthors, 2013: African tropical rainforest net carbon dioxide fluxes in the twentieth century. *Philos. Trans. Roy. Soc.*, **368B**, 20120376, https://doi.org/10.1098/rstb.2012.0376.

Gerber, S., L. O. Hedin, S. G. Keel, S. W. Pacala, and E. Shevliakova, 2013: Land use change and nitrogen feedbacks constrain the trajectory of the land carbon sink. *Geophys. Res. Lett.*, **40**, 5218–5222, https://doi.org/10.1002/grl.50957.

Juang, J.-Y., G. Katul, M. Siqueira, P. Stoy, and K. Novick, 2007: Separating the effects of albedo from eco-physiological changes on surface temperature along a successional chronosequence in the southeastern United States. *Geophys. Res. Lett.*, **34**, L21408, https://doi.org/10.1029/2007GL031296.

Khanna, J., D. Medvigy, S. Fueglistaler, and R. Walko, 2017: Regional dry-season climate changes due to three decades of Amazonian deforestation. *Nat. Climate Change*, **7**, 200–204, https://doi.org/10.1038/nclimate3226.

Laguë, M. M., and A. L. Swann, 2016: Progressive midlatitude afforestation: Impacts on clouds, global energy transport, and precipitation. *J. Climate*, **29**, 5561–5573, https://doi.org/10.1175/JCLI-D-15-0748.1.

Lawrence, D., and K. Vandecar, 2015: Effects of tropical deforestation on climate and agriculture. *Nat. Climate Change*, **5**, 27–36, https://doi.org/10.1038/nclimate2430.

Lawrence, D. M., and Coauthors, 2016: The Land Use Model Intercomparison Project (LUMIP) contribution to CMIP6: Rationale and experimental design. *Geosci. Model Dev.*, **9**, 2973–2998, https://doi.org/10.5194/gmd-9-2973-2016.

Lee, X., and Coauthors, 2011: Observed increase in local cooling effect of deforestation at higher latitudes. *Nature*, **479**, 384–387, https://doi.org/10.1038/nature10588.

Li, Y., M. Zhao, S. Motesharrei, Q. Mu, E. Kalnay, and S. Li, 2015: Local cooling and warming effects of forests based on satellite observations. *Nat. Commun.*, **6**, 6603, https://doi.org/10.1038/ncomms7603.

——, N. de Noblet-Ducoudré, E. L. Davin, S. Motesharrei, N. Zeng, S. C. Li, and E. Kalnay, 2016: The role of spatial scale and background climate in the latitudinal temperature response to deforestation. *Earth Syst. Dyn.*, **7**, 167–181, https://doi.org/10.5194/esd-7-167-2016.

Lorenz, R., A. J. Pitman, and S. A. Sisson, 2016: Does Amazonian deforestation cause global effects; can we be sure? *J. Geophys. Res. Atmos.*, **121**, 5567–5584, https://doi.org/10.1002/2015JD024357.

Luyssaert, S., and Coauthors, 2014: Land management and land-cover change have impacts of similar magnitude on surface temperature. *Nat. Climate Change*, **4**, 389–393, https://doi.org/10.1038/nclimate2196.

Mahmood, R., and Coauthors, 2014: Land cover changes and their biogeophysical effects on climate. *Int. J. Climatol.*, **34**, 929–953, https://doi.org/10.1002/joc.3736.

McNaughton, K. G., and T. W. Spriggs, 1986: A mixed-layer model for regional evaporation. *Bound.-Layer Meteor.*, **34**, 243–262, https://doi.org/10.1007/BF00122381.

Medvigy, D., R. L. Walko, and R. Avissar, 2012: Simulated links between deforestation and extreme cold events in South America. *J. Climate*, **25**, 3851–3866, https://doi.org/10.1175/JCLI-D-11-00259.1.

Mullens, T. J., 2013: Evaluation and improvements of the offline CLM4 using ARM data. M.S. thesis, Dept. of Meteorology and Climate Science, San Jose State University, 80 pp., scholarworks.sjsu.edu/cgi/viewcontent.cgi?article=7903&context=etd_theses.

Murray-Tortarolo, G., and Coauthors, 2013: Evaluation of land surface models in reproducing satellite-derived LAI over the high-latitude Northern Hemisphere. Part I: Uncoupled DGVMs. *Remote Sens.*, **5**, 4819–4838, https://doi.org/10.3390/rs5104819.

Neale, R. B., and Coauthors, 2012: Description of the NCAR Community Atmosphere Model (CAM 5.0). NCAR/TN-486+STR, 274 pp., www.cesm.ucar.edu/models/cesm1.0/cam/docs/description/cam5_desc.pdf.

Piao, S., and Coauthors, 2013: Evaluation of terrestrial carbon cycle models for their response to climate variability and to

CO_2 trends. *Global Change Biol.*, **19**, 2117–2132, https://doi.org/10.1111/gcb.12187.

Pielke, R. A., and Coauthors, 2011: Land use/land cover changes and climate: Modeling analysis and observational evidence. *Wiley Interdiscip. Rev.: Climate Change*, **2**, 828–850, https://doi.org/10.1002/wcc.144.

Pitman, A. J., and R. Lorenz, 2016: Scale dependence of the simulated impact of Amazonian deforestation on regional climate. *Environ. Res. Lett.*, **11**, 094025, https://doi.org/10.1088/1748-9326/11/9/094025.

——, and Coauthors, 2009: Uncertainties in climate responses to past land cover change: First results from the LUCID intercomparison study. *Geophys. Res. Lett.*, **36**, L14814, https://doi.org/10.1029/2009GL039076.

Quesada, B., A. Arneth, and N. de Noblet-Ducoudré, 2017: Atmospheric, radiative, and hydrologic effects of future land use and land cover changes: A global and multimodel climate picture. *J. Geophys. Res. Atmos.*, **122**, 5113–5131, https://doi.org/10.1002/2016JD025448.

Riahi, K., and Coauthors, 2011: RCP 8.5—A scenario of comparatively high greenhouse gas emissions. *Climatic Change*, **109**, 33–57, https://doi.org/10.1007/s10584-011-0149-y.

Rigden, A. J., and D. Li, 2017: Attribution of surface temperature anomalies induced by land use and land cover changes. *Geophys. Res. Lett.*, **44**, 6814–6822, https://doi.org/10.1002/2017GL073811.

Rotenberg, E., and D. Yakir, 2011: Distinct patterns of changes in surface energy budget associated with forestation in the semiarid region. *Global Change Biol.*, **17**, 1536–1548, https://doi.org/10.1111/j.1365-2486.2010.02320.x .

Schimel, D., B. B. Stephens, and J. B. Fisher, 2015: Effect of increasing CO_2 on the terrestrial carbon cycle. *Proc. Natl. Acad. Sci. USA*, **112**, 436–441, https://doi.org/10.1073/pnas.1407302112.

Snyder, P. K., C. Delire, and J. A. Foley, 2004: Evaluating the influence of different vegetation biomes on the global climate. *Climate Dyn.*, **23**, 279–302, https://doi.org/10.1007/s00382-004-0430-0.

Swann, A. L., I. Y. Fung, and J. C. Chiang, 2012: Mid-latitude afforestation shifts general circulation and tropical precipitation. *Proc. Natl. Acad. Sci. USA*, **109**, 712–716, https://doi.org/10.1073/pnas.1116706108.

Thiery, W., E. L. Davin, H. J. Panitz, M. Demuzere, S. Lhermitte, and N. van Lipzig, 2015: The impact of the African Great Lakes on the regional climate. *J. Climate*, **28**, 4061–4085, https://doi.org/10.1175/JCLI-D-14-00565.1.

Vanden Broucke, S., S. Luyssaert, E. L. Davin, I. Janssens, and N. van Lipzig, 2015: New insights in the capability of climate models to simulate the impact of LUC based on temperature decomposition of paired site observations. *J. Geophys. Res. Atmos.*, **120**, 5417–5436, https://doi.org/10.1002/2015JD023095.

von Randow, C., and Coauthors, 2004: Comparative measurements and seasonal variations in energy and carbon exchange over forest and pasture in South West Amazonia. *Theor. Appl. Climatol.*, **78**, 5–26, https://doi.org/10.1007/s00704-004-0041-z.

Wilks, D. S., 2006: On "field significance" and the false discovery rate. *J. Appl. Meteor. Climatol.*, **45**, 1181–1189, https://doi.org/10.1175/JAM2404.1.

Winckler, J., C. H. Reick, and J. Pongratz, 2017: Robust identification of local biogeophysical effects of land-cover change in a global climate model. *J. Climate*, **30**, 1159–1176, https://doi.org/10.1175/JCLI-D-16-0067.1.

Zhang, M., and Coauthors, 2014: Response of surface air temperature to small-scale land clearing across latitudes. *Environ. Res. Lett.*, **9**, 034002, https://doi.org/10.1088/1748-9326/9/3/034002.

Zhao, L., X. Lee, R. B. Smith, and K. Oleson, 2014: Strong contributions of local background climate to urban heat islands. *Nature*, **511**, 216–219, https://doi.org/10.1038/nature13462.

Zwiers, F. W., and H. von Storch, 1995: Taking serial correlation into account in tests of the mean. *J. Climate*, **8**, 336–351, https://doi.org/10.1175/1520-0442(1995)008<0336:TSCIAI>2.0.CO;2.